Improving the Generality of the Fictitious Magnetic Charge Approach to Computing Inductances in the Presence of Permeable Materials

Yehia Massoud
Synopsys Inc.
Mountain View, CA

Jacob White
MIT
Cambridge, MA

ABSTRACT

In this paper we present an improvement to the fictitious magnetic charge approach to computing inductances in the presence of permeable materials. The improvement replaces integration over a "non-piercing" surface with a line integral and an efficient quadrature scheme. Eliminating the need to generate non-piercing surfaces substantially simplifies handling problems with general geometries of permeable materials. Computational results are presented to demonstrate the accuracy and versatility of the new method.

Categories and Subject Descriptors

G.4 [Mathematical Software]: Algorithm design and analysis; G.1.2 [Approximation]: Approximation of surfaces and contours

General Terms

Algorithms

1. INTRODUCTION

Improvements in fabrication technology is making it possible to use permeable materials in a variety of micromachined devices (or MEMS), and designers are exploiting these materials to increase magnetic force or inductance while preserving small device size [1, 2, 3, 4, 5, 6, 7]. However, the planar nature of most micromachining technology implies that designers can not simply wrap coils of wire around highly permeable cores. Instead, the geometric freedom available results in designs that are difficult to analyze analytically, making numerical extraction tools essential.

One approach to computing inductance in the presence of permeable materials is the fictitious magnetic charge method [8, 9], in which permeable material interfaces are replaced with fictitious sheets of magnetic charge. The fictitious magnetic charges are then determined by enforcing continuity of normal magnetic fields at the permeable material interfaces.
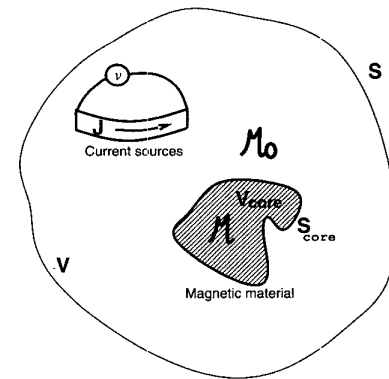
Figure 1: Current sources are outside the magnetic material

The method is accurate, even for highly permeable materials, because fields are never computed inside those permeable materials. However, there is also a difficulty. In order to use the fictitious magnetic charge method it is necessary to construct a surface which bounds the current carrying conductors and does not penetrate the permeable material. Constructing "non-piercing" surfaces for arbitrary geometries of conductors and permeable material structures is very difficult.

In this paper we show that the fictitious magnetic charge method can be modified, eliminating the need for the non-piercing surfaces. In Section 2, we briefly describe the integral formulation of the fictitious magnetic charge method and its use of non-piercing surfaces. In Section 3, we present a new method which uses line integrals and quadrature schemes. In Section 4, we give computational results to demonstrate the accuracy of our approach. Finally, in Section 5, we summarize the work presented in the paper.

2. FORMULATION BACKGROUND

For many problems in MEMS, one can assume that the permeable materials do not conduct current and are separated from conductors, as shown in Figure 1. For such problems it is possible to derive an integral formulation for the conductor currents based on introducing fictitious magnetic charge at permeable material interfaces [8]. Using this
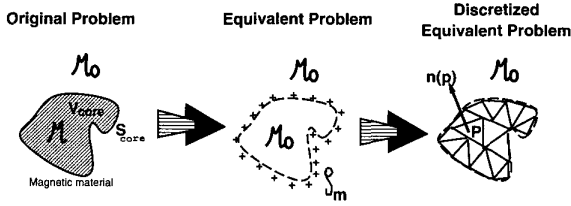
Figure 2: Linear magnetic material can be represented with an equivalent free space problem with magnetic surface charges distributed on the magnetic material interfaces. The interface is discretized into panels on which charge is assumed constant

approach the magnetic problem becomes equivalent to the free space problem, as shown in Figure 2. The fictitious magnetic charge can be determined from the equation for the jump in the normal magnetic field at the permeable material interface as in,

$$\rho_m(r)\frac{2\pi(\mu_r+1)}{(\mu_r-1)} = \nabla \times \int_v \frac{J(r')dv' \cdot n(r)}{|r-r'|} - \int_s \rho_m(r')n(r) \cdot \nabla \frac{1}{|r-r'|}dS'_{core} \quad (1)$$

where ρ_m is the fictitious surface charge density, S_{core} is the surface of the magnetic material, μ_r is the magnetic material's relative permeability, J is the current density, and n(r) is the unit vector normal to the magnetic material surface calculated at point r. Note that the second term of (1) represents the normal magnetic field due to currents, and the third term represents the normal magnetic field due to fictitious magnetic charges.

The conductor currents satisfy an integral equation derived using a vector potential generated by the conductor currents and the fictitious magnetic charges,

$$\frac{J(r)}{\sigma} + \frac{j\omega\mu}{4\pi} \int_V' \frac{J(r')}{|r-r'|}dv' + \frac{j\omega\mu}{4\pi} \nabla_r \int_{S'_m} \frac{-\rho_m(r')}{|r-r'|}dS'_m = -\nabla \phi(r) \quad (2)$$

where S_m is the surface of the permeable material, and ϕ is the scalar potential. Note that the second term and the third term of (2), divided by $j\omega\mu$, represent the vector potential due to the currents and the the vector potential due to fictitious magnetic charges, respectively.

In order to solve these two coupled integral equations (1) and (2), the surface of the magnetic material is discretized into panels and the current carrying conductors are sliced into filaments that are then combined into loops. Using these so-generated loop and panel basis functions converts the integral equations (1) and (2) to a linear system of equations [8]:

$$\begin{bmatrix} R(\omega) + j\omega L_J(\omega) & j\omega L_\rho(\omega) \\ Hn_J & (Hn_\rho - I) \end{bmatrix} \begin{bmatrix} \bar{I}_M \\ \bar{q}_m \end{bmatrix} = \begin{bmatrix} V \\ 0 \end{bmatrix} \quad (3)$$

where I_M, V, and q_m are vectors of loop currents, loop voltages, and fictitious magnetic charge densities, respectively. The sub-matrices R, L_J, Hn_ρ and Hn_J are computed using techniques described in [8, 9].
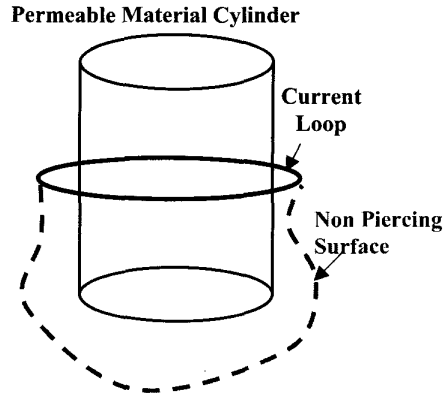

Figure 3: A non Piercing current loop surface. The surface should avoid cutting the permeable material in order to avoid numerical cancellation errors.

2.1 Evaluating $[L_\rho]_{ki}$

The matrix element $[L_\rho]_{ki}$ corresponds to the impact of magnetic charge on panel k on the current in loop i and is given by:

$$[L_\rho]_{ki} = -\frac{j\omega\mu_0}{4\pi} \int_{S_{loop\ i}} \nabla \frac{1}{|r-r'|} \cdot n(r)dS, \quad (4)$$

where n(r) is the normal to the surface of current loop i at point r and $S_{loop\ i}$ is the non-piercing surface bounded by the filaments in loop i. In order to avoid numerical cancellation errors, the surface should be non-piercing. That is, the surface should not penetrate the magnetic material, as shown in Figure 3.

The integral in (4) comes from integrating $1/r$ over the surface bounded by the filaments in current loop i and evaluating the result at a point at the permeable material surface. For simple configurations of current carrying conductors and permeable materials, one can find a non-piercing surface like the tented one shown in Figure 4. This tented surface can then be divided into triangles, and therefore, $[L_\rho]_{ki}$ can be expressed as:

$$[L_\rho]_{ki} = -\frac{j\omega\mu_0}{4\pi} \sum_\Delta \int_{S_\Delta} \nabla_r \frac{1}{|r-r'|} \cdot n(\Delta)dS_\Delta \quad (5)$$

where S_Δ is a triangle on the current loop surface, and $n(\Delta)$ is the normal to triangle on the current loop (loop) surface. The integral inside the summation in (5) is the potential due to a dipole charge distribution on a triangles which can be evaluated analytically [10].

3. IMPROVING THE EVALUATION OF $[L_\rho]_{KI}$

In this section, we show the improvement we have made to calculation of the $[L_\rho]_{ki}$ integral using line integration. This avoids the problem of finding and constructing non-piercing surfaces which can be very difficult and sometimes impossible for a range of MEMS devices such multiple turn spiral inductors. Also, this method facilitates the automation of inductance extraction using the fictitious magnetic charge no matter how complicated is the configuration of the current carrying conductors or the permeable structures.
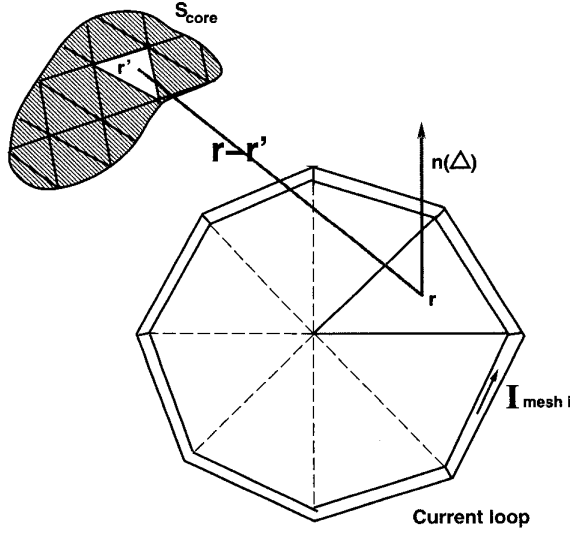
553

Figure 4: Evaluating $[L_\rho]_{ki}$, the effect of the magnetic charge on panel k on the current in loop i. Note that the surface of the current loop i is divided into triangles.

Figure 5: Evaluating of the solid angle integral at the origin P_0

Consider translating the surface of the loop to a new coordinate system such that the center of panel k is the origin of the new coordinate system, P_0. Thus, the integral in (4) becomes

$$[L_\rho]_{ki} = \frac{j\omega\mu_0}{4\pi} \int_{S_{loop\ i}} \frac{1}{r^2} [u_r \cdot n(r)] dS \qquad (6)$$

where $n(r)$ is the normal to the surface of current loop i at point r and u_r is the unit vector along the r direction. The integral in (6) is equal to $\frac{j\omega\mu_0}{4\pi} I_\Omega(P_0)$, where $I_\Omega(P_0)$ is the solid angle integral. The solid angle integral is dependent only on the contour of the surface [11]. The solid angle integral $I_\Omega(P_0)$ is given by

$$I_\Omega(P_0) = \frac{1}{4\pi} \oint_C \left[\frac{Z(l)}{R(l)} - 1 \right] \frac{(\hat{\rho} \cdot \hat{v})(\hat{t} \cdot \hat{\eta})}{\rho} dL \qquad (7)$$

where R and Z are the two spherical coordinates of the point l on contour C, ρ is the projection of vector R on the x-y plane, $\hat{\rho}$ is the unit vector along ρ, $\hat{t}$ and $\hat{\eta}$ are the unit tangential vectors of the contour C and the projection curve of C on x-y plane, respectively, and $\hat{v} = \hat{\eta} \times \hat{z}$ with $\hat{z}$ being a unit vector along the z-axis. The geometry is shown in Figure 5.

Now we use the idea of the solid angle to get an efficient way to calculate $[L_\rho]_{ki}$. After translating the surface of the loop to a new coordinate system such that the center of panel k is the origin of the new coordinate system, P_0, $[L_\rho]_{ki}$ can be calculated as in

$$[L_\rho]_{ki} = \sum_{f=1}^{\#filaments\ in\ loop\ i} E_{kf} =$$

$$\frac{j\omega\mu_0}{4\pi} \sum_{f=1}^{\#fil.in\ loop\ i} \int_{L_{fil_f}} \left[\frac{Z(l)}{R(l)} - 1 \right] \frac{(\hat{\rho} \cdot \hat{v})(\hat{t} \cdot \hat{\eta})}{\rho} dL \qquad (8)$$
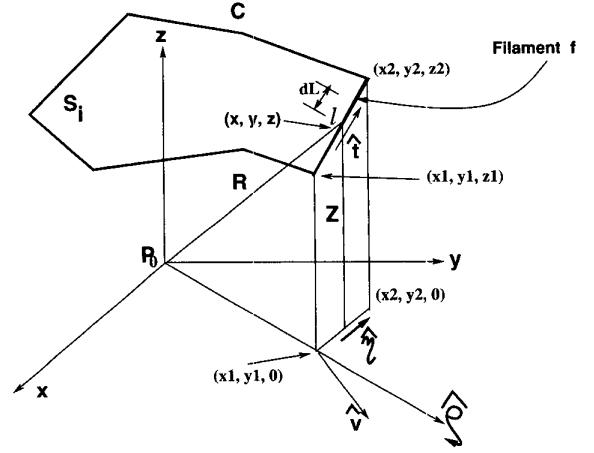
After some mathematical manipulation, we get an expression for E_{kf} as in

$$E_{kf} = \frac{j\omega\mu_0}{4\pi} \int_l \left[\frac{z}{\sqrt{x^2 + y^2 + z^2}} - 1 \right] *$$

$$\left[\frac{x(y_2 - y_1) - y(x_2 - x_1)}{(x^2 + y^2)} \right] *$$

$$\left[\frac{1}{(x_2 - x_1)^2 + (y_2 - y_1)^2 + (z_2 - z_1)^2} \right] dL \qquad (9)$$

where dL is a line integral along filament f,

$$x = x_1 + \left[\frac{(x_2 - x_1) * L}{(x_2 - x_1)^2 + (y_2 - y_1)^2 + (z_2 - z_1)^2} \right],$$

$$y = y_1 + \left[\frac{(y_2 - y_1)) * L}{(x_2 - x_1)^2 + (y_2 - y_1)^2 + (z_2 - z_1)^2} \right],$$

and

$$z = z_1 + \left[\frac{(z_2 - z_1)) * L}{(x_2 - x_1)^2 + (y_2 - y_1)^2 + (z_2 - z_1)^2} \right]$$

Note that (x_1, y_1, z_1) is the translated starting point of filament f and (x_2, y_2, z_2) is the translated end point of filament f, as shown in Figure 5.

The integral in (9) has a smooth integrand and can be computed easily using numerical quadrature [12]. We, thus, efficiently evaluate the elements of L_ρ in the linear system (3).

4. COMPUTATIONAL RESULTS

In order to demonstrate the accuracy and the versatility of the improved fictitious magnetic surface charge method, we used the improved method to solve for the frequency dependent inductance of a realistic spiral inductor over a permeable material substrate, as shown in Figure 6.

The new technique computes integrals using the line integral over the length of the spiral and avoids generating non-piercing surfaces. The tested realistic spiral inductor in Figure 6 has a diameter of 280μ, with a 10μ by 10μ cross section. The permeable material substrate is 1500μ by 1500μ,
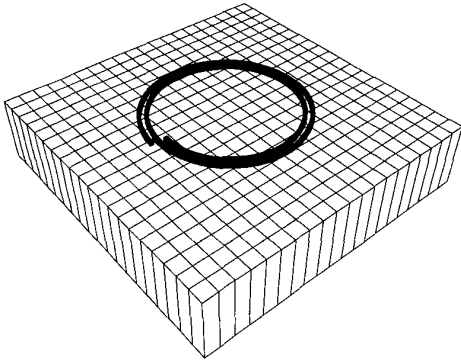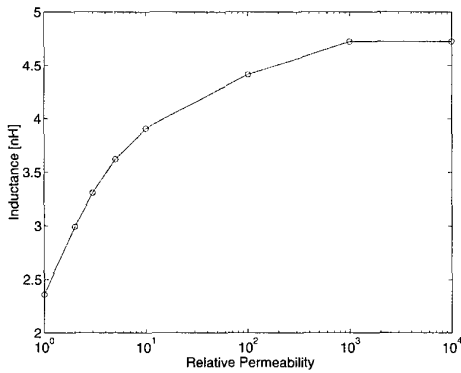
Figure 6: A spiral inductor over a magnetic substrate.

Figure 7: Variation of the inductance of spiral inductor with relative of the magnetic substrate.

Figure 8: Inductance frequency response of the spiral inductor over a magnetic substrate example. The substrate has a relative permeability of 2000.

with 200μ as its thickness. Figure 7 shows the variation of extracted inductance with the permeability of the permeable substrate. The inductance of the spiral inductor over a magnetic substrate increases as the permeability increases, till it reaches an upper limit which is almost double the value of the spiral inductance without a substrate. This agrees very well with the theoretical analysis in [13]. Figure 8 shows the frequency response of the inductance of the spiral inductor in Figure 6. Note the high frequency inductance is lower than the low frequency one, due to the skin effect.

5. CONCLUSIONS AND ACKNOWLEDGMENTS

An improved method for extracting frequency dependent inductances in the presence of permeable materials has been presented. The method eliminates the need to generate non-piercing surfaces, and is easily applied to general three-dimensional problems. Results were presented to demonstrate the accuracy and versatility of the new method.

The authors would like to acknowledge the support of the Advanced Technology Group at Synopsys, as well as support from the DARPA MEMS program, the National Science Foundation, and the Semiconductor Research Corporation.
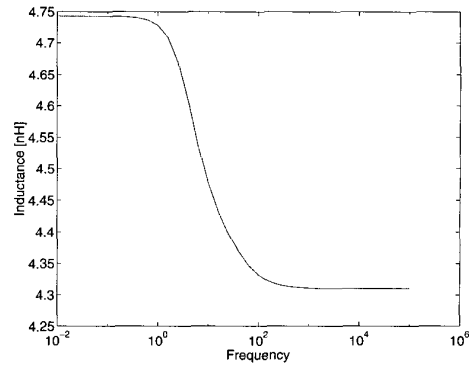
6. REFERENCES

[1] H. Guckel, T. Christenson, K. Skrobis, T. Jung, J. Klein, K. Hartojo, and I. Widjaja, "A first functional current excited planar rotational magnetic micromotor," *IEEE Transactions on Micro-Electromechanical Systems*, pp. 7–11, January 1993.

[2] C. Ahn and M. Allen, "Micromachined planar inductors on silicon wafers for mems applications," *IEEE Transactions on Industrial Electronics*, pp. 866–876, December 1998.

[3] W. Taylor, O. Brand, and M. Allen, "Fully integrated magnetically actuated micromachined relays," *Journal of Microelectromechanical Systems*, pp. 181–191, June 1998.

[4] C. Ahn and M. Allen, "A planar micromachined spiral inductor for integrated magnetic microactuator applications," *Journal of Micromechanics and Microengineering*, pp. 37–44, June 1993.

[5] C. Sullivan and S. Sanders, "Design of microfabricated transformers and inductors for high-frequency power conversion," *IEEE Transactions on Power Electronics*, pp. 228–238, February 1996.

[6] T. Sato, H. Tomita, A. Sawabe, T. Inoue, T. Mizoguhci, and M. Sahashi, "A magnetic thin film inductor and its application to a MHZ switching dc-dc converter," *IEEE Transactions on Micro-Electromechanical Systems*, pp. 217–223, March 1994.

[7] K. Yamaguchi, E. Sugawara, O. Nakajima, and H. Matsuki, "Load characteristics of a spiral inductor type thin film microtransformers," *IEEE Transactions on Magnetics*, pp. 3207–3209, June 1993.

[8] Y. Massoud and J. White, "Fast inductance extraction of 3-d structures with non-const permeabilities," in *Proceedings of the International Conference on Modeling and Simulation of Microsystems*, April 1998.

[9] Y. Massoud, J. Wang, and J. White, "Accurate inductance extraction with permeable materials using qualocation," in *Proceedings of the International Conference on Modeling and Simulation of Microsystems*, April 1999.

[10] J. N. Newman, "Distributions of sources and normal dipoles over a quadrilateral panel," *Journal of Engineering Mathematics*, vol. 20, no. 2, pp. 113–126, 1986.

[11] Y. Liu, "Analysis of shell-like structures by the boundary element method based on 3-d elasticity: formulation and verification," *International Journal for Numerical Methods in Engineering*, vol. 41, pp. 541–558, 1998.

[12] D. Engels, *Numerical Quadrature and Cubature.* New York: Academic Press, 1980.

[13] W. Roshen and D. Turcotte, "Effect of finite thickness of magnetic substrate on planar inductors," *IEEE Transactions on Magnetics*, pp. 270–275, January 1990.